

SiCL: Silhouette-Driven Contrastive Learning for Unsupervised Person Re-Identification with Clothes Change

Mingkun Li^{†,1}, Peng Xu^{*,2}, Chun-Guang Li^{†,1}, Jun Guo^{†,1}

¹Beijing University of Posts and Telecommunications, ²Tsinghua University

[†]{mingkun.li, lichunguang, guojun}@bupt.edu.cn, ^{*}peng_xu@tsinghua.edu.cn

Abstract

In this paper, we address a highly challenging yet critical task: unsupervised long-term person re-identification with clothes change. Existing unsupervised person re-id methods are mainly designed for short-term scenarios and usually rely on RGB cues so that fail to perceive feature patterns that are independent of the clothes. To crack this bottleneck, we propose a silhouette-driven contrastive learning (SiCL) method, which is designed to learn cross-clothes invariance by integrating both the RGB cues and the silhouette information within a contrastive learning framework. To our knowledge, this is the first tailor-made framework for unsupervised long-term clothes change re-id, with superior performance on six benchmark datasets. We conduct extensive experiments to evaluate our proposed SiCL compared to the state-of-the-art unsupervised person re-id methods across all the representative datasets. Experimental results demonstrate that our proposed SiCL significantly outperforms other unsupervised re-id methods.

1. Introduction

Person re-identification (re-id) aims to match person identities of bounding box images that are captured from distributed camera views [35]. Most conventional studies for unsupervised person re-id have only focused on the scenarios *without* clothes change [7, 37]. However, re-id in such scenarios is unrealistic since people may often change their clothing. Thus, these studies for the scenarios *without* clothes change may only be useful in the short-term re-id settings but fail to handle the long-term person re-id for which we have to face the scenarios with clothes changes.

Recently, there have been some attempts to address the long-term re-id task [11, 33]. However, all of these attempts employ supervised learning methods which heavily rely on large amounts of labelled training data. Unfortunately, collecting and annotating person identity labels under the scenario of unconstrained clothes change is ex-

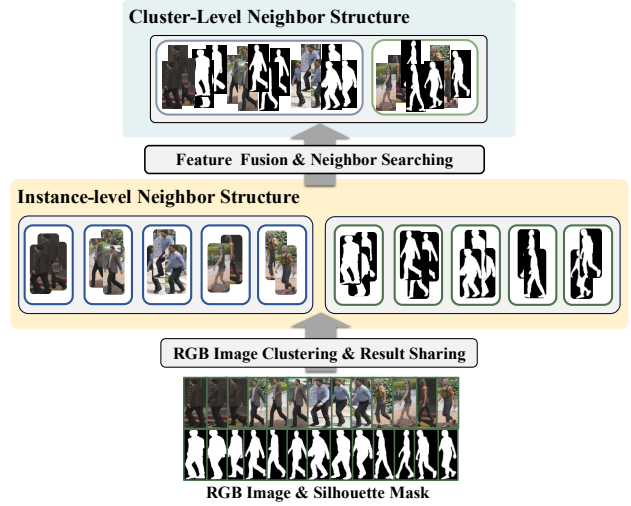


Figure 1. Illustration of hierarchical fusion clustering: At a lower level, clustering is used to reveal the neighbor structure of instances. At a higher level, silhouette features and RGB features are integrated to exploit the neighbor structure of the clusters.

tremely difficult. Preparing labelled re-id training data, e.g., DeepChange [32], in a realistic scenario is quite expensive and exhausting.

Due to the significance of long-term person re-id, it is appealing to develop unsupervised method to address long term person re-id problem without the tedious requirement of person identity labeling. This is a more complex but more realistic extension of the previous unsupervised short-term person re-id [8, 21, 22] that different people may have similar clothes whilst the same person might wear variant clothes with very distinct appearances, as shown in Fig. 2. Unfortunately, prior investigations on unsupervised person re-identification have neglected situations involving clothing changes. Conventional approaches are incapable of capturing clothing-independent patterns since they solely rely on RGB features as their driving force [20]. Specifically, the majority of existing unsupervised methods [5] are

cluster-oriented and tend to yield feature extractions primarily dominated by color [20].

As a consequence, the clustering algorithm will blindly assign every training sample with a color-based pseudo label, which is error-prone with a large cumulative propagation risk and ultimately leads to sub-optimal solutions, such as simply grouping the individuals who wear the same clothing.

In this paper, we propose a novel silhouette-driven contrastive learning framework, termed SiCL, for attacking the challenging task of unsupervised person re-id in long-term setting. In SiCL, we incorporate the person silhouette and RGB images into a contrastive learning framework to learn cross-clothes invariance features. Specifically, SiCL employs a dual-branch network to perceive both silhouette and RGB image features and incorporates them to construct a hierarchical neighbor structure, as demonstrated in Fig. 1. The RGB feature is used to construct the low-level instance neighbor structure, and the fused features are used to construct the high-level cluster neighbor structure. Different from other methods that are only relying on RGB patterns to construct the single-level neighbor structure, in SiCL, we incorporate clothing-independent features hidden in the silhouette. Such an additional feature can provide further guidance to modeling the invariant features across different clothes. Moreover, we introduce a contrast-learning module to learn invariant features between the silhouette and RGB images at various neighbor structure levels.

To validate the effectiveness of our SiCL approach, we conduct comprehensive evaluation on six long-term person re-id datasets comparing to the state-of-the-art unsupervised person re-identification (re-id) methods. Experimental results demonstrate the superior performance of our approach. Notably, our SiCL can not only outperforms all short-term methods significantly, but also achieves comparable performance to the the state-of-the-art fully supervised methods.

The main contribution of the paper can be summarized as follows.

1. We propose a silhouette-driven contrastive learning framework for unsupervised long-term person re-id with clothes change. To the best of our knowledge, this is the first work to investigate unsupervised long-term person re-id with clothes change.
2. We propose to incorporate both person silhouette information and hierarchical neighbor structure into a contrastive learning framework to guide the model for learning cross-clothes invariance feature.
3. We conduct extensive experiments on six representative datasets to evaluate the performance of the proposed SiCL and the state-of-the-art unsupervised re-id methods.



Figure 2. Visualizing the intrinsic challenges in long-term person re-id with clothes change. We randomly selected 28 images of a single individual from the DeepChange [32] dataset. Evidently, the variances in visual characteristics between different outfits (rows) are considerably more pronounced compared to those within the same outfit (each column).

2. Related Work

2.1. Long-Term Person Re-Identification

A few recent person re-id studies attempt to tackle [31, 33] the long-term clothes-changing situations via supervised training, and emphasize the use of additional supervision for the general appearance features (e.g., clothes, color), to enable the model to learn the cross-clothes features. For example, [33] generates contour sketch images from RGB images and highlights the invariance between the sketch and RGB. [11] explores fine-grained body shape features by estimating masks with discriminative shape details and extracting pose-specific features. While these seminal works provide inspiring attempts for re-id with clothes change, there are still some limitations: a) Generating contour sketches or other side-information requires additional model components and will cause extra computational cost; b) To the best of our knowledge, all models designed for re-id clothes change are supervised learning methods, and thus lack of generalization ability to the open-world dataset settings. In this paper, we attempt to tackle the challenging re-id with clothes change under unsupervised setting.

2.2. Unsupervised Person Re-Identification

To avoid the high consumption in data labeling, a large and growing body of literature has investigated unsupervised person re-id [30, 38]. The existing unsupervised person Re-ID methods can be divided into two categories: a) unsupervised domain adaptation methods, which require a labeled source dataset and an unlabelled target dataset [25, 30]; and b) purely unsupervised methods that work with only an unlabelled dataset [3, 5]. However, up to date, the unsupervised person re-id methods are focusing on short-term scenarios, none of them taking into account the long-term re-id scenario. To the best of our knowledge, this is the first attempt to address the long-term person re-id in unsupervised setting. Thus, as a byproduct, we systematically and comprehensively evaluate the performance of the existing the state-of-the-art unsupervised methods [3, 8] on six long-term person re-id datasets and set up a preliminary benchmarking ecosystem for the long-term person re-id commu-

nity.

3. Our Methodology: Silhouette-Driven Contrastive Learning (SiCL)

Our SiCL approach integrates silhouette and RGB images into a contrastive learning framework assisted with the guidance from hierarchical clustering structure. For clarity, we provide a flowchart of our SiCL in Fig. 3. Our SiCL consists of two network branches: $F(\cdot|\Theta)$ and $F'(\cdot|\Theta')$, which perceive RGB and silhouette patterns, respectively. We use Θ and Θ' to denote the corresponding network parameters. In our SiCL, the parameters Θ and Θ' are learned separately (without parameters sharing). We design a predictor layer $G(\cdot|\Psi)$ which follows the RGB branch, where Ψ denotes the parameters in the predictor layer. In addition, we also design a feature fusion layer $R(\cdot|\Omega)$, where Ω denotes the parameters.

Given an unlabeled pedestrian image dataset $\mathcal{I} = \{I_i\}_{i=1}^N$ consisting of N samples, we generate the corresponding pedestrian silhouette mask dataset $\mathcal{S} = \{S_i\}_{i=1}^N$ through human parsing network such as SCHP [23]. For an input image $I_i \in \mathcal{I}$, we use the I_i as the input of $F(\cdot|\Theta)$ and S_i as the inputs of $F'(\cdot|\Theta')$. For simplicity, we denote the output features of the $F(\cdot|\Theta)$ and $F'(\cdot|\Theta')$ as \mathbf{x}_i and $\tilde{\mathbf{x}}_i$, denote the output of the predictor layer in the $G(\cdot|\Psi)$ as \mathbf{z}_i , and denote the output of fusion layer $R(\cdot|\Omega)$ as \mathbf{f}_i , where $\mathbf{x}_i, \tilde{\mathbf{x}}_i, \mathbf{z}_i, \mathbf{f}_i \in R^D$.

As illustrated in Fig. 3, our SiCL compose of a contrastive learning module and a hierarchical fusion clustering module. In hierarchical fusion clustering module, the hierarchical neighbor structure is generated by leveraging RGB and silhouette features at both the instance-level and cluster-level. In contrastive learning module, we introduce the person’s silhouette and use the hierarchical neighbor structure as supervision information to train model, and investigate cross-clothes features via contrastive learning. Furthermore, we build an adaptive learning strategy to automatically modify the hierarchical neighbor selection, which can flexibly select neighbor clusters according to dynamic criteria.

To store the outputs of the two branches and the fusion layer, in SiCL, we maintain the three instance-memory banks $\mathcal{M} = \{\mathbf{v}_i\}_{i=1}^N$, $\tilde{\mathcal{M}} = \{\tilde{\mathbf{v}}_i\}_{i=1}^N$, and $\hat{\mathcal{M}} = \{\hat{\mathbf{v}}_i\}_{i=1}^N$, respectively, where $\mathbf{v}_i, \tilde{\mathbf{v}}_i, \hat{\mathbf{v}}_i \in R^D$. Memory banks \mathcal{M} and $\hat{\mathcal{M}}$ are initialized with $\mathcal{X} := \{\mathbf{x}_1, \dots, \mathbf{x}_N\}$ and $\tilde{\mathcal{M}}$ is initialized with $\tilde{\mathcal{X}} := \{\tilde{\mathbf{x}}_1, \dots, \tilde{\mathbf{x}}_N\}$, where \mathcal{X} and $\tilde{\mathcal{X}}$ are the outputs of $F(\cdot|\Theta)$ and $F'(\cdot|\Theta')$.

3.1. Hierarchical Fusion Clustering

To construct a hierarchical neighbor structure, we sort the hierarchical neighbor structure into two levels: a) low-level instance neighbors, and b) high-level cluster neighbors.

Low-level Instance Neighbors. We use $F(\cdot|\Theta)$ outputs to construct m clusters $\mathcal{C} := \{\mathcal{C}^{(1)}, \mathcal{C}^{(2)}, \dots, \mathcal{C}^{(m)}\}$. The clustering result \mathcal{C} indicates the connection between neighbors at the instance level since that if samples are clustered together, it also indicates that their RGB features are similar. In the subsequent training process, this clustering result \mathcal{C} will also be used to guide the training of branch $F'(\cdot|\Theta')$.

High-level Cluster Neighbors. Since that the silhouette masks contain richer clothing invariance features, we use them to find those pedestrian samples that are similar at the cluster level, e.g., the same person wearing different clothing. To be specific, we fuse the RGB feature and the silhouette feature to renew the representation of instance, and search the cluster neighbor based on fusion features. For an image \mathbf{I}_i , the fusion feature \mathbf{f}_i is defined as:

$$\mathbf{f}_i = F(\text{concat}(\mathbf{x}_i|\tilde{\mathbf{x}}_i)), \quad (1)$$

where $\text{concat}(\cdot)$ denotes the channel-wise concatenating \mathbf{x}_i and $\tilde{\mathbf{x}}_i$. Based on the fused features, we define the cluster center $\mathbf{u}_{\omega(\mathbf{I}_i)}$ as

$$\mathbf{u}_{\omega(\mathbf{I}_i)} = \frac{1}{|\mathcal{C}^{(\omega(\mathbf{I}_i))}|} \sum_{I_j \in \mathcal{C}^{(\omega(\mathbf{I}_i))}} \mathbf{f}_j, \quad (2)$$

where $\omega(\mathbf{I}_i)$ is the cluster index of image \mathbf{I}_i .

Once constructing the cluster centre $U = \{\mathbf{u}_i\}_{i=1}^m$, we will find the cluster-level nearest neighbours based on the similarity of the cluster centres. Once contrasting the cluster-center, we find cluster-level neighbors and construct the neighbor set \mathcal{N} . Specifically, for cluster $\mathcal{C}^{(\ell)}$, we define the similarity between clusters $\mathcal{C}^{(\ell)}$ and $\mathcal{C}^{(i)}$ as

$$\mathcal{D}(\mathcal{C}^{(\ell)}, \mathcal{C}^{(i)}) = \frac{\mathbf{u}_\ell^\top \mathbf{u}_i}{\|\mathbf{u}_\ell\|_2 \|\mathbf{u}_i\|_2}. \quad (3)$$

We denote the cluster neighbor set of cluster $\mathcal{C}^{(\ell)}$ as $\mathcal{N}^{(\ell)}$, which includes the top- k similar clusters $\mathcal{C}^{(i)}$ sorted by $\mathcal{D}(\mathcal{C}^{(\ell)}, \mathcal{C}^{(i)})$. Then, we form the total cluster-level neighbor set $\mathcal{A} := \{\mathcal{N}^{(1)}, \dots, \mathcal{N}^{(m)}\}$. This process is known as hierarchical fusion clustering due to the use of a fused feature operation and the construction of a multi-level neighbor structure.

In the hierarchical fusion clustering stage, we construct neighbor structures based on some specific clustering algorithm and cluster-level neighbor searching, respectively. The clustering result of the output features $\mathcal{X} := \{\mathbf{x}_1, \dots, \mathbf{x}_N\}$ from $F(\cdot|\Theta)$ is used to generate the pseudo labels $\mathcal{Y} := \{y_1, \dots, y_N\}$, and cluster-level neighbor set \mathcal{A} contains the neighbor index for each cluster. In the contrastive learning stage, the hierarchical neighbor structure is used as supervision information to guide the model learn cross-clothes features.

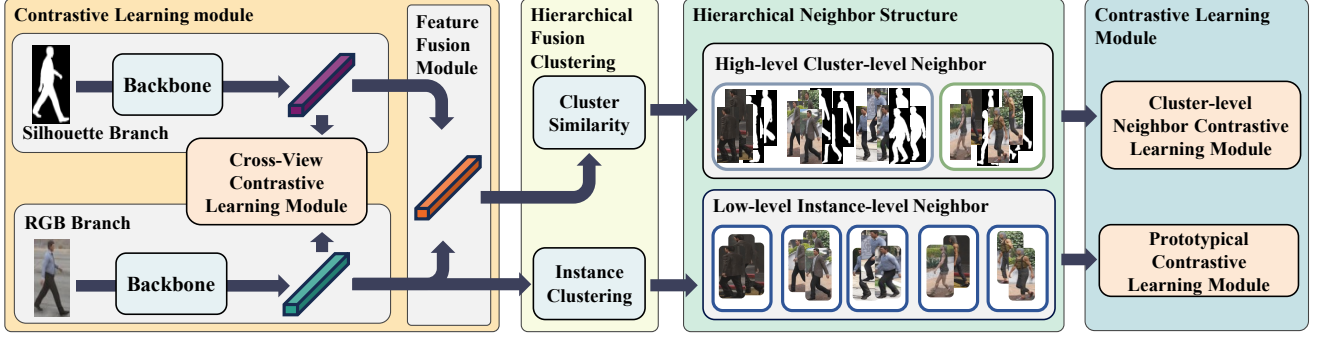


Figure 3. Our proposed Silhouette-Driven Contrastive Learning (SiCL) framework.

3.2. Contrastive Learning Module

To effectively explore the invariance features between RGB images and silhouette masks, we construct three contrastive learning modules to train SiCL assisted with the self-supervision information provided by the hierarchical fusion clustering as follows: a) Prototypical contrastive learning module, which is used for contrast training between positive samples and negative pairs; b) Cross-view contrastive learning module, which is used for contrast training between RGB images and silhouette masks; and c) Cluster-level neighbor contrastive learning module, which is used for contrast training between cluster-level neighbor clusters and negative pairs.

Prototypical Contrastive Learning Module. We apply prototypical contrastive learning to discover the hidden information inside the cluster structure. For the i -th instance, we denote its cluster index as $\omega(I_i)$, the center of $C^{\omega(I_i)}$ as the positive prototype, and all other cluster centers as the negative prototypes. We define the prototypical contrastive learning loss as follows:

$$\mathcal{L}_P = - \sum_{q^* \in \{q, \tilde{q}, \hat{q}\}} (1 - q_i^*)^2 \ln(q_i^*), \quad (4)$$

where q_i , \tilde{q}_i and \hat{q}_i measure the consistency between the outputs of $F(\cdot|\Theta)$, $F'(\cdot|\Theta')$ and $R(\cdot|\Omega)$ and the related prototype computed with the memory bank and are defined as

$$q_i = \frac{\exp(\mathbf{p}_{\omega(I_i)}^\top \mathbf{x}_i / \tau)}{\sum_{\ell=1}^m \exp(\mathbf{p}_\ell^\top \mathbf{x}_i / \tau)}, \quad (5)$$

where $\mathbf{p}_{\omega(I_i)}$ as the RGB prototype vector of the cluster $C^{\omega(I_i)}$ is defined by

$$\mathbf{p}_{\omega(I_i)} = \frac{1}{|\mathcal{C}^{\omega(I_i)}|} \sum_{I_j \in \mathcal{C}^{\omega(I_i)}} \mathbf{v}_j, \quad (6)$$

here \mathbf{v}_j is the instance feature of image I_j in \mathcal{M} , $\tilde{\mathbf{p}}_i$ and $\hat{\mathbf{p}}_i$ are calculated in the same way with corresponding instance memory bank $\hat{\mathcal{M}}$ and $\tilde{\mathcal{M}}$, respectively.

The prototypical contrastive learning module performs contrastive learning between positive and negative prototypes to improve the discriminant ability for the networks $F(\cdot|\Theta)$ and $F'(\cdot|\Theta')$ and the feature fusion layer $R(\cdot|\Omega)$.

Cross-view Contrastive Learning Module. To effectively train the contrastive learning framework across the two views, we design a cross-view contrastive module to mine the invariance between RGB images and silhouette masks. To match the feature outputs of two network branches at both the instance level and cluster level, specifically, we introduce the negative cosine similarity of the outputs of $G(\cdot|\Psi)$ and $F'(\cdot|\Theta')$ to define the two-level contrastive losses as follows:

$$\mathcal{L}_C := - \frac{\mathbf{z}_i^\top \tilde{\mathbf{x}}_i}{\|\mathbf{z}_i\|_2 \|\tilde{\mathbf{x}}_i\|_2} - \frac{\mathbf{z}_i^\top \tilde{\mathbf{p}}_{\omega(I_i)}}{\|\mathbf{z}_i\|_2 \|\tilde{\mathbf{p}}_{\omega(I_i)}\|_2}, \quad (7)$$

where $\|\cdot\|_2$ is the ℓ_2 -norm.

The cross-view contrastive learning module explores the invariance between RGB images and silhouette masks and thus assist the network to mine the invariance information provided by the RGB image and the silhouette mask, as well as imposing such a self-supervision information on the module for learning clothing-unrelated features.

Cluster-level Neighbor Contrastive Learning Module. To avoid training the model into degeneration that only push samples with similar appearance together, we design a cluster-level neighbor contrastive learning module. Particularly, we propose a weighted cluster-level neighbor contrastive loss as follows:

$$\mathcal{L}_N = - \sum_{j \in \mathcal{N}^{\omega(I_i)}} w_{ij} \left(\frac{\mathbf{z}_i^\top \tilde{\mathbf{p}}_j}{\|\mathbf{z}_i\|_2 \|\tilde{\mathbf{p}}_j\|_2} \right), \quad (8)$$

where $\mathcal{N}^{\omega(I_i)}$ is the set of neighbors of cluster $\omega(I_i)$, and w_{ij} is the weight, which is defined as

$$w_{ij} = \mathcal{D}(\mathcal{C}^{(i)}, \mathcal{C}^{(j)}), \quad (9)$$

in which $\mathcal{D}(\mathcal{C}^{(i)}, \mathcal{C}^{(j)})$ is defined in Eq. 3. Owing to the Cluster-level neighbor contrastive learning module trained

via loss in Eq. 8, the cluster-level neighbors will be pushed closer in the feature space. This will help the model to investigate consistency across different neighbor clusters.

3.3. Curriculum Nerighbour Selecting

Since in the early training stages, the model has a weaker ability to distinguish samples, we hope the ability improves during training. To this end, we provide a curriculum strategy for searching neighbors which sets the search range according to the training progress. Specifically, we set the cluster-level neighbor searching range k as

$$k := t \lfloor K/T \rfloor, \quad (10)$$

where T is the total number of training epochs and t is the current step, K is a hyper-parameter.

3.4. Training and Inference Procedure for SiCL

Training Procudure. In SiCL, the two branches are implemented with ResNet-50 [10] and do not share the parameters. We first pre-train the two network branches on ImageNet and use the learned features to initialize the three memory banks \mathcal{M} , $\tilde{\mathcal{M}}$, and $\hat{\mathcal{M}}$, respectively. In the training phase, we train both network branches and the fusion layer with loss:

$$\mathcal{L} := \mathcal{L}_P + \mathcal{L}_C + \mathcal{L}_N. \quad (11)$$

We update the three instance memory banks \mathcal{M} , $\tilde{\mathcal{M}}$ and $\hat{\mathcal{M}}$, respectively, as follows:

$$\mathbf{v}_i^{(t)} \leftarrow \alpha \mathbf{v}_i^{(t-1)} + (1 - \alpha) \mathbf{x}_i, \quad (12)$$

where $\tilde{\mathbf{v}}_i^{(t)}$ and $\hat{\mathbf{v}}_i^{(t)}$ unpdate in the same way, and α is set as 0.2 by default.

In implementation, we use DBSCAN algorithm [6] to generate the raw clusters. DBSCAN is a density-based clustering algorithm. It regards a data point as density reachable if the data point lies within a small distance threshold d to other samples, where the parameter d is the distance threshold to find neighboring point.

Inference Procedure. After training, we keep only the ResNet $F(\cdot|\Theta)$ in for inference. We compute the distances between each image in the query and each image in the gallery using the feature obtained from the output of the first branch $F(\cdot|\Theta)$. We then sort the distances in ascending order to discover the matched results.

4. Experiments

4.1. Experimental Setting

Datasets. We evaluate SiCL on six clothes change re-id datasets: LTCC [33], PRCC [34], VC-Clothes [29], Celeb-ReID [15], Celeb-ReID-Light [14] and DeepChange [32]. Table 1 shows an overview of dataset in details.

Algorithm 1 SiCL algorithm

Input: Image \mathcal{I} and Silhouette \mathcal{S} ;

Parameter: Cluster distance d , Neighbor Searching Range K ;

Output: P_{best}

- 1: Pre-train the two network branches on ImageNet;
 - 2: Initialize the instance memory banks \mathcal{M} , $\tilde{\mathcal{M}}$, $\hat{\mathcal{M}}$ and set $P = P_{best} = 0$;
 - 3: **while** epoch \leq total epoch **do**
 - 4: Perform feature extraction to get \mathcal{X} , $\tilde{\mathcal{X}}$ and $\hat{\mathcal{X}}$;
 - 5: Perform clustering on \mathcal{X} to yield m clusters $\mathcal{C} := \{\mathcal{C}^{(1)}, \mathcal{C}^{(2)}, \dots, \mathcal{C}^{(m)}\}$;
 - 6: Generate cluster-level neighbor set \mathcal{A} through Eq 3;
 - 7: Train SiCL with supervised infromation provided by \mathcal{A} and \mathcal{C} , i.e., updating Θ , Ψ , Ω and Θ' via the total loss in Eq. 11;
 - 8: Update instance memory bank \mathcal{M} , $\tilde{\mathcal{M}}$ and $\hat{\mathcal{M}}$ via Eq. 12;
 - 9: Evaluate the model performance P with $F(\cdot|\Theta)$;
 - 10: **if** $P > P_{best}$ **then**
 - 11: Output the best model $F(\cdot|\Theta)$ and set $P_{best} \leftarrow P$;
 - 12: **end if**
 - 13: **end while**
 - 14: **return** P_{best} .
-

Protocols and Metrics. Different from the traditional short-term person re-id setting, there are two evaluation protocols for long-term person re-id: a) general setting and b) clothes-change setting. Specifically, for a query image, the general setting is looking for cross-camera matching samples of the same identity, while the clothes-change setting additionally demands the same identity with inconsistent clothing. For LTCC [33] and PRCC [34], we report performance with both clothes-change setting and general setting. As for Celeb-ReID [15], Celeb-ReID-Light [14] DeepChange [32] and VC-Clothes [29], we report the general setting performance. We use both Cumulated Matching Characteristics (CMC) and mean average precision (mAP) as retrieval accuracy metrics.

Implementation Details. In SiCL, we use ResNet-50 [10] pre-trained on ImageNet [19] for both network branches. The features dimension $D = 2048$. We use the output \mathbf{x}_i of the first branch $F(\cdot|\Theta)$ to perform clustering, where $\mathbf{x}_i \in \mathbb{R}^D$. The prediction layer $G(\cdot|\Psi)$ is a $D \times D$ full connection layer, the fusion layer $R(\cdot|\Omega)$ is a $2D \times D$ full connection layer. The cluster distance $d = 0.6$ for PRCC, LTCC, Celeb-ReID and Celeb-ReID-Light datasets, and $d = 0.7$ for VC-Clothes. We optimize the network through Adam optimizer [18] with a weight decay of 0.0005 and train the network with 60 epochs in total. The learning rate is initially set as 0.00035 and decreased to one-tenth per 20 epochs. The batch size is set to 64. The temperature

Dataset	Size	Subset			Identity	Camera	Clothes
		Train	Query	Gallery			
DeepChange	178, 407	75, 083	17, 527	62, 956	1, 121	17	-
LTCC	17, 119	9, 576	493	7, 050	152	12	14
PRCC	33, 698	17, 896	3, 543	12, 259	221	3	-
Celeb-ReID	34, 186	20, 208	2, 972	11, 006	1, 052	-	-
Celeb-ReID-Light	10, 842	9, 021	887	934	590	-	-
VC-Clothes	19, 060	9, 449	1, 020	8, 591	256	4	3

Table 1. Long-term Person Re-ID Datasets details.

Method	Reference	LTCC				PRCC					
		C-C		General		C-C		General			
		mAP	R-1	mAP	R-1	mAP	R-1	R-10	mAP	R-1	R-10
Supervised Method(ST-ReID)											
HACNN	CVPR'18	9.30	21.6	26.7	60.2	-	21.8	59.4	-	82.5	98.1
PCB	ECCV'18	10.0	23.5	30.6	38.7	38.7	22.8	61.4	97.0	86.8	99.8
Supervised Method(LT-ReID)											
CESD	ACCV'20	12.4	26.2	34.3	71.4	-	-	-	-	-	-
RGA-SC	CVPR'20	14.0	31.4	27.5	65.0	-	42.3	79.4	-	98.4	100
IANet	CVPR'19	12.6	25.0	31.0	63.7	45.9	46.3	-	98.3	99.4	-
GI-ReID	CVPR'22	10.4	23.7	29.4	63.2	-	-	-	-	-	-
RCSANet	CVPR'21	-	-	-	-	48.6	50.2	-	97.2	100	-
3DSL	CVPR'21	14.8	31.2	-	-	-	51.3	-	-	-	-
FSAM	CVPR'21	16.2	28.5	25.4	73.2	-	54.5	86.4	-	98.8	100
CAL	CVPR'22	18.0	40.1	40.8	74.2	55.8	55.2	-	99.8	100	-
CCAT	IJCNN'22	19.5	29.1	50.2	87.2	-	69.7	89.0	-	96.2	100
Unsupervised Method											
SpCL	NeurIPS'20	7.60	15.3	21.2	47.3	45.2	33.2	71.3	90.6	86.4	98.3
C3AB	PR'22	8.30	15.2	20.7	46.7	48.6	36.7	74.0	90.2	88.3	98.1
CACL	TIP'22	6.20	9.80	22.3	45.6	52.1	41.7	79.8	94.7	90.9	99.9
CC	ACCV'22	6.00	7.40	11.0	17.0	46.3	34.4	74.4	94.4	90.2	99.9
ICE	ICCV'21	7.10	14.5	28.4	61.1	48.0	34.8	74.2	95.9	93.6	99.9
ICE*	ICCV'21	10.1	16.3	22.6	44.0	45.5	32.6	72.3	95.7	93.3	99.8
PPLR	CVPR'22	4.40	4.80	6.00	11.2	51.4	40.0	75.2	91.7	87.4	99.8
SiCL	Ours	10.1	20.7	27.6	57.6	55.4	43.2	80.2	96.2	93.8	99.4

Table 2. Comparison with the state-of-the-art methods on LTCC and PRCC, ‘C-C’ means clothes change setting, ‘General’ means general setting. ‘*’ means using the camera label as side-information.

coefficient τ in Eq. 5 is set to 0.05 and the update factor α in Eq. 12 is set to 0.2. The K in Eq. 10 is set as 10 on LTCC, Celeb-ReID and Celeb-ReID-Light, 3 on VC-Clothes and 5 on PRCC, the effect of using a different value of K will be test later.¹

4.2. Comparison to State-of-the-art Methods

Competitors. To construct a preliminary benchmark and conduct a thorough comparison, we evaluate some the state-of-the-art of short-term unsupervised re-id mod-

els, which are able to achieve competitive performance under an unsupervised short-term setting, including SpCL [8], CC [4], CACL [20], C3AB [22], ICE [1], PPLR [3]. We retrain and evaluate these unsupervised methods on long-term datasets, including LTCC, PRCC, Celeb-ReID, Celeb-ReID-Light and VC-Clothes. At the same time, we also compare with other supervised long-term person re-id methods such as HACNN [24], PCB [28], CESD [26], RGA-SC [36], IANet [13], GI-ReID [17], RCSANet [16], 3DSL [2], FSAM [12], CAL [9], CCAT [27]. The comparison results of the state-of-the-art unsupervised short-term person re-id methods and supervised methods are shown in

¹The code for the work will be released upon the acceptance of the paper.

Method	Reference	VC-Clothes			
		C-C		General	
		mAP	R-1	mAP	R-1
Supervised Method(ST-ReID)					
PCB	ECCV'18	30.9	34.5	83.3	86.2
Supervised Method(LT-ReID)					
HACNN	CVPR'18	62.2	62.0	94.3	94.7
RGA-SC	CVPR'20	67.4	71.1	94.8	95.4
FSAM	CVPR'21	78.9	78.6	94.8	94.7
CCAT	IJCNN'22	76.8	83.5	85.5	92.7
Unsupervised Method					
SpCL	NeurIPS'20	38.2	46.2	61.0	77.8
C3AB	PR'22	44.1	52.0	65.0	81.0
CACI	TIP'22	49.7	58.9	68.0	82.4
CC	ACCV'22	25.7	31.0	45.1	62.4
ICE	ICCV'21	28.7	34.5	51.2	69.3
ICE*	ICCV'21	28.5	31.4	51.8	70.1
PPLR	CVPR'22	23.1	32.5	47.7	68.1
SiCL	Ours	63.9	71.7	77.2	87.9

Table 3. Comparison on VC-Clothes.

Method	Reference	Celeb-ReID		Celeb-Light	
		mAP	R-1	mAP	R-1
Supervised Method(ST-ReID)					
TS	TOMM'17	7.80	36.3	-	-
Supervised Method(LT-ReID)					
MLFN	CVPR'18	6.00	41.4	6.30	10.6
HACNN	CVPR'18	9.50	47.6	11.5	16.2
PA	ECCV'18	6.40	19.4	-	-
PCB	ECCV'18	8.20	37.1	-	-
MGN	MM'18	10.8	49.0	13.9	21.5
DG-Net	CVPR'19	10.6	50.1	12.6	23.5
Celeb	IJCNN'19	-	-	14.0	26.8
Re-IDCaps	TCSVT'19	9.80	51.2	11.2	20.3
RCSANet	CVPR'21	11.9	55.6	16.7	29.5
Unsupervised Method					
SpCL	NeurIPS'20	4.60	39.6	3.60	5.30
C3AB	PR'22	4.80	41.0	3.70	5.10
CACL	TIP'22	5.10	42.3	3.60	4.30
CC	ACCV'22	3.40	32.8	3.20	4.40
ICE	ICCV'21	4.90	40.7	5.00	7.10
PPLR	CVPR'22	4.80	41.3	4.30	6.20
SiCL	Ours	5.60	45.4	5.60	10.5

Table 4. Comparison with the state-of-the-art methods on Celeb-ReID and Celeb-ReID-Light.

Tables 2, 4 and 3. From the results in these tables we can read that our SiCL outperforms much better than all unsupervised short-term methods and even comparable to some supervised long-term methods.

Method	VC		PRCC		LTCC	
	mAP	R-1	mAP	R-1	mAP	R-1
C-C						
Single*	44.4	54.0	48.4	37.7	9.20	17.1
Baseline	62.8	71.4	54.2	42.5	9.80	18.6
SiCL	63.9	71.7	55.4	43.2	10.1	20.7

Table 5. Ablation Study on LTCC, PRCC and VC-Clothes, Single* means only use RGB images in training without contrastive learning.

Particularly, we can observe that SiCL yields much higher performance than the short-term unsupervised person re-id methods in clothes-change setting. Yet, the differences are reduced and even vanished in general settings (e.g., ICE results on LTCC). This further demonstrates the dependency of short-term re-id methods on clothes features for person matching. In addition, we discovered that SiCL performs poorly on certain datasets, such as Celeb-ReID-Light; we will investigate the underlying causes in *Supplementary Material*.

4.3. Ablation Study

In this section, we conduct a series of ablation experiments to evaluating each component in SiCL architecture, i.e., contrastive learning framework, the neighbor contrastive learning module \mathcal{L}_N , separately. In addition, we substitute the feature fusion operation with different branch feature.

Baseline Setting. In the baseline network, we employ the prototypical contrastive learning module and the cross-view contrastive learning module and train the model with the corresponding loss functions. The training procedure and memory updating strategy are kept the same as SiCL.

The ablation study results are presented Table 5. We can read that when each component is added separately, the performance increases. This verifies that each component contributes to improved performance.

Other Experiments. We have provided more comprehensive and complex results of the ablation experiments in the *Supplementary Material*, including the range of neighbour search K , the clustering distance parameter d , and others.

4.4. More Evaluations and Analysis

Different Operations for Cluster-level Neighbor Searching. To determine the requirement of feature fusion, we prepare a set of tests employing different operations, i.e. using x and \tilde{x} , to find the cluster neighbors. The experimental results are listed in Table 10. We can read that only using \tilde{x} in the cluster neighbor searching stage will also yield acceptable performance in finding cluster neighbors. This observation confirms that rich information on the high-level neighbor structure may be gleaned using just a silhouette source. However, the results obtained from the LTCC

Operation	VC		PRCC		LTCC	
	mAP	R-1	mAP	R-1	mAP	R-1
C-C						
x	61.8	69.4	55.1	42.9	10.4	21.4
\tilde{x}	63.6	71.4	53.8	42.4	10.9	21.9
SiCL	63.9	71.7	55.4	43.2	10.1	20.7

Table 6. Experiments Results of Various Cluster Neighbor Searching Operations on LTCC, PRCC, and VC-Clothes.

Method	Backbone	DeepChange		
		mAP	R-1	R-10
Supervised Method				
DeepChange	ResNet-50	9.62	36.6	55.5
DeepChange	ReIDCaps	13.2	44.2	62.0
DeepChange	ViT B16	14.9	47.9	67.3
Unsupervised Method				
SpCL	ResNet-50	8.90	32.9	47.2
SiCL	ResNet-50	12.4	41.0	56.0

Table 7. Experimental Results on DeepChange.

dataset indicate that the feature fusion operations did not yield optimal performance. The rationales behind this observation will be elaborated upon in the supplementary materials.

Performance Evaluation on DeepChange. DeepChange is the latest, largest, and realistic person re-id benchmark with clothes change. We conduct experiments to evaluate the performance of SiCL and SpCL on this dataset, and report the results in Table 7. Moreover, we also listed the results of supervised training methods using the different backbones provided by DeepChange [32].

5. Conclusion

We have addressed a challenging task: unsupervised long-term person re-id with clothes change. Specifically, we proposed a silhouette-driven contrastive learning approach, termed SiCL, which takes the silhouette masks into contrastive learning and constructs a hierarchically neighborhood structure to facilitate the training. By leveraging the silhouette feature and the hierarchical neighborhood relationship, SiCL is able to effectively exploit the invariance within and between RGB images and silhouette masks to learn more effective cross-clothes features. We conducted extensive experiments on six widely-used re-id datasets with clothes change. Experimental results demonstrated the superiority of our proposed approach. To the best of our knowledge, this is the first time that the unsupervised long-term person re-id problem has been tackled. In addition, our systematic evaluations can serve as a benchmark for the unsupervised long-term person re-id community.

References

- [1] Hao Chen, Benoit Lagadec, and Francois Bremond. Ice: Inter-instance contrastive encoding for unsupervised person re-identification. In *ICCV*, pages 14960–14969, 2021. 6
- [2] Jiaying Chen, Xinyang Jiang, Fudong Wang, Jun Zhang, Feng Zheng, Xing Sun, and Wei-Shi Zheng. Learning 3d shape feature for texture-insensitive person re-identification. In *CVPR*, pages 8146–8155, 2021. 6
- [3] Yoonki Cho, Woo Jae Kim, Seunghoon Hong, and Sung-Eui Yoon. Part-based pseudo label refinement for unsupervised person re-identification. In *CVPR*, pages 7308–7318, 2022. 2, 6
- [4] Zuozhuo Dai, Guangyuan Wang, Siyu Zhu, Weihao Yuan, and Ping Tan. Cluster contrast for unsupervised person re-identification. *arXiv preprint arXiv:2103.11568*, 2021. 6
- [5] Zuozhuo Dai, Guangyuan Wang, Weihao Yuan, Siyu Zhu, and Ping Tan. Cluster contrast for unsupervised person re-identification. In *ACCV*, pages 1142–1160, 2022. 1, 2
- [6] Martin Ester, Hans-Peter Kriegel, Jörg Sander, and Xiaowei Xu. A density-based algorithm for discovering clusters in large spatial databases with noise. In *SIGKDD*, 1996. 5
- [7] Yixiao Ge, Zhuowan Li, Haiyu Zhao, Guojun Yin, Shuai Yi, Xiaogang Wang, and Hongsheng Li. Fd-gan: Pose-guided feature distilling gan for robust person re-identification. In *NeurIPS*, 2018. 1
- [8] Yixiao Ge, Feng Zhu, Dapeng Chen, Rui Zhao, and Hongsheng Li. Self-paced contrastive learning with hybrid memory for domain adaptive object re-id. In *NeurIPS*, 2020. 1, 2, 6
- [9] Xinqian Gu, Hong Chang, Bingpeng Ma, Shutao Bai, Shiguang Shan, and Xilin Chen. Clothes-changing person re-identification with rgb modality only. In *CVPR*, pages 1060–1069, 2022. 6
- [10] Kaiming He, Xiangyu Zhang, Shaoqing Ren, and Jian Sun. Deep residual learning for image recognition. In *CVPR*, 2016. 5
- [11] Peixian Hong, Tao Wu, Ancong Wu, Xintong Han, and Wei-Shi Zheng. Fine-grained shape-appearance mutual learning for cloth-changing person re-identification. In *CVPR*, 2021. 1, 2
- [12] Peixian Hong, Tao Wu, Ancong Wu, Xintong Han, and Wei-Shi Zheng. Fine-grained shape-appearance mutual learning for cloth-changing person re-identification. In *CVPR*, pages 10513–10522, 2021. 6
- [13] Ruibing Hou, Bingpeng Ma, Hong Chang, Xinqian Gu, Shiguang Shan, and Xilin Chen. Interaction-and-aggregation network for person re-identification. In *CVPR*, pages 9317–9326, 2019. 6
- [14] Yan Huang, Qiang Wu, Jingsong Xu, and Yi Zhong. Celebrities-reid: A benchmark for clothes variation in long-term person re-identification. In *IJCNN*, pages 1–8. IEEE, 2019. 5
- [15] Yan Huang, Jingsong Xu, Qiang Wu, Yi Zhong, Peng Zhang, and Zhaoxiang Zhang. Beyond scalar neuron: Adopting vector-neuron capsules for long-term person re-identification. *TCSVT*, 30(10):3459–3471, 2019. 5

- [16] Yan Huang, Qiang Wu, JingSong Xu, Yi Zhong, and ZhaoXiang Zhang. Clothing status awareness for long-term person re-identification. In *ICCV*, pages 11895–11904, 2021. 6
- [17] Xin Jin, Tianyu He, Kecheng Zheng, Zhiheng Yin, Xu Shen, Zhen Huang, Ruoyu Feng, Jianqiang Huang, Zhibo Chen, and Xian-Sheng Hua. Cloth-changing person re-identification from a single image with gait prediction and regularization. In *CVPR*, pages 14278–14287, 2022. 6
- [18] Diederik P. Kingma and Jimmy Ba. Adam: A method for stochastic optimization. In *3rd International Conference on Learning Representations*, 2015. 5
- [19] Alex Krizhevsky, Ilya Sutskever, and Geoffrey E Hinton. Imagenet classification with deep convolutional neural networks. In *NeurIPS*, 2012. 5
- [20] Mingkun L, Li Chun-Guang, and Jun Guo. Cluster-guided asymmetric contrastive learning for unsupervised person re-identification. *TIP*, 2022. 1, 2, 6
- [21] Minxian Li, Xiatian Zhu, and Shaogang Gong. Unsupervised person re-identification by deep learning tracklet association. In *ECCV*, 2018. 1
- [22] Mingkun Li, He Sun, Chaoqun Lin, Chun-Guang Li, and Jun Guo. The devil in the tail: Cluster consolidation plus cluster adaptive balancing loss for unsupervised person re-identification. *PR*, 129:108763, 2022. 1, 6
- [23] Peike Li, Yunqiu Xu, Yunchao Wei, and Yi Yang. Self-correction for human parsing. *TPAMI*, 2020. 3
- [24] Wei Li, Xiatian Zhu, and Shaogang Gong. Harmonious attention network for person re-identification. In *CVPR*, pages 2285–2294, 2018. 6
- [25] Peixi Peng, Tao Xiang, Yaowei Wang, Massimiliano Pontil, Shaogang Gong, Tiejun Huang, and Yonghong Tian. Unsupervised cross-dataset transfer learning for person re-identification. In *CVPR*, 2016. 2
- [26] Xuelin Qian, Wenxuan Wang, Li Zhang, Fangrui Zhu, Yanwei Fu, Tao Xiang, Yu-Gang Jiang, and Xiangyang Xue. Long-term cloth-changing person re-identification. In *ACCV*, 2020. 6
- [27] Xuena Ren, Dongming Zhang, and Xiuguo Bao. Person re-identification with a cloth-changing aware transformer. In *2022 International Joint Conference on Neural Networks (IJCNN)*, pages 1–8. IEEE, 2022. 6
- [28] Yifan Sun, Liang Zheng, Yi Yang, Qi Tian, and Shengjin Wang. Beyond part models: Person retrieval with refined part pooling (and a strong convolutional baseline). In *ECCV*, pages 480–496, 2018. 6
- [29] Fangbin Wan, Yang Wu, Xuelin Qian, Yixiong Chen, and Yanwei Fu. When person re-identification meets changing clothes. In *CVPRW*, 2020. 5
- [30] Jingya Wang, Xiatian Zhu, Shaogang Gong, and Wei Li. Transferable joint attribute-identity deep learning for unsupervised person re-identification. In *CVPR*, 2018. 2
- [31] Kai Wang, Zhi Ma, Shiyan Chen, Jinni Yang, Keke Zhou, and Tao Li. A benchmark for clothes variation in person re-identification. *IJIS*, 2020. 2
- [32] Peng Xu and Xiatian Zhu. Deepchange: A long-term person re-identification benchmark with clothes change. In *Proceedings of the IEEE international conference on computer vision (ICCV)*, 2023. 1, 2, 5, 8
- [33] Qize Yang, Ancong Wu, and Wei-Shi Zheng. Person re-identification by contour sketch under moderate clothing change. *TPAMI*, 2019. 1, 2, 5
- [34] Qize Yang, Ancong Wu, and Wei-Shi Zheng. Person re-identification by contour sketch under moderate clothing change. *TPAMI*, 2019. 5
- [35] Mang Ye, Jianbing Shen, Gaojie Lin, Tao Xiang, Ling Shao, and Steven CH Hoi. Deep learning for person re-identification: A survey and outlook. *arXiv preprint arXiv:2001.04193*, 2020. 1
- [36] Zhizheng Zhang, Cuiling Lan, Wenjun Zeng, Xin Jin, and Zhibo Chen. Relation-aware global attention for person re-identification. In *CVPR*, pages 3186–3195, 2020. 6
- [37] Rui Zhao, Wanli Oyang, and Xiaogang Wang. Person re-identification by saliency learning. *TPAMI*, 2016. 1
- [38] Liang Zheng, Yi Yang, and Alexander G Hauptmann. Person re-identification: Past, present and future. *arXiv preprint arXiv:1610.02984*, 2016. 2

SiCL: Silhouette-Driven Contrastive Learning for Unsupervised Person Re-Identification with Clothes Change

Supplementary Material

In the supporting materials, we provide the implementation details of the experiments, such as evaluations on using different K , d , and a set of visualization results. Besides, we also discuss the limitation and the future work.

6. Implementation Details and Supplementary Experiments

6.1. Implementation Details

Our experiments are implemented with PyTorch and run on a server equipped with an Intel(R) Xeon(R) CPU E5-2630-v4 and four Nvidia 3090 GPUs of memory 24 GB. The contrastive learning framework is based on CACL.

6.2. More Evaluation and Analysis

Ablation Study on Celeb-ReID and Celeb-ReID-Light . The ablation study results are presented in Table 9. We can read that when each component is added separately, the performance increases. This verifies that each component contributes to improved performance.

Performance on Celeb-ReID-Light. For the LTCC, PRCC, and VC-Clothes datasets, SiCL does not vary substantially from the supervised methods; however, the difference is apparent on the Celeb-ReID-Light dataset. Due to the small size of the Celeb-ReID-Light dataset, the look of the same person apparel differs substantially while including just one picture per clothing type. This is a significant difficulty for the clustering-based methods, as it is difficult for the model to accurately recognize the same pedestrians wearing various garments during training.

Evaluation on Parameters in DBSCAN. We conduct experiments on LTCC and VC-Clothes to evaluate the effects of changing the parameter d . Experiments are recorded in Table 8. we can find that while $d = 0.6$, SiCL demonstrates the highest performance on LTCC. We can observe that SiCL is comparatively sensitive to d . This suggests that SiCL is somewhat reliant on the quality of the clustering. This is because if the clustering quality is low, the instance neighbor information will also be in error. Such errors can cumulatively at the clustering level, which negatively impacts the model training. Therefore, one of our forthcoming research directions is to make SiCL less sensitive to the clustering parameter in the future.

Different operations for cluster-level neighbor searching. To determine the requirement of feature fusion, we prepare a set of tests employing different operations, such as using x , \tilde{x} , to find the cluster-level neighbors. The exper-

Table 8. Performance Comparison of different cluster parameter d (the maximum distance between neighbor points) on SiCL.

Eps	VC-Clothes		LTCC	
	mAP	R-1	mAP	R-1
General				
0.8	8.70	15.7	4.30	9.90
0.7	77.2	87.9	11.8	25.2
0.6	76.5	87.4	27.6	57.6
0.5	70.4	82.8	22.9	46.5
0.4	64.3	78.0	18.7	43.6

Method	Celeb-ReID		Celeb-ReID-Light	
	mAP	R-1	mAP	R-1
C-C				
Single*	4.80	40.5	5.00	8.50
Baseline	5.60	44.2	5.20	10.0
SiCL	6.00	45.0	5.40	9.50

Table 9. Ablation Study on Celeb-ReID and Celeb-ReID-Light, Single* means only use RGB images in training without contrastive learning.

Operation	VC		PRCC		LTCC	
	mAP	R-1	mAP	R-1	mAP	R-1
C-C						
Baseline	62.8	71.4	54.2	42.5	9.80	18.6
x	61.8	69.4	54.1	42.4	10.4	20.4
\tilde{x}	63.6	71.4	54.6	42.6	10.5	20.9
SiCL	63.9	71.7	55.4	43.2	10.1	20.7

Table 10. Experiments Results of Various Cluster-Level Neighbor Searching Operations on LTCC, PRCC, and VC-Clothes.

imental results are listed in Table 10. We can find that using only \tilde{x} during the cluster-level neighbour searching stage also yield satisfactory results. Conversely, using only x to search the cluster-level neighbor would have a detrimental effect on the model performance on both VC-Clothes and PRCC. This observation confirms that rich clothes-independent information can be gleaned by just using the silhouette feature.

Performance with different K . Table 11 illustrates the effect of varying cluster-level neighbor search parameters K across various datasets. We can find that our SiCL is not sensitive to the change of the cluster-level neighbor search parameter K on PRCC. However, for the VC-

K	VC-Clothes				PRCC	
	C-C		General		C-C	
	mAP	R-1	mAP	R-1	mAP	R-1
10	63.9	71.7	77.2	87.9	54.4	42.6
8	63.4	71.2	76.8	87.7	55.2	43.8
6	62.5	70.0	75.5	86.9	54.5	42.5
4	63.0	70.5	77.2	87.1	54.1	43.1
2	63.1	69.8	74.5	86.1	54.6	42.8

Table 11. Illustration for the model performance with different K on PRCC and VC-Clothes.

Clothes dataset, when the neighbour search range is less than 6, the cluster-level neighbour information seems to play a negative role and does not bring any performance improvement to the model. We believe that this problem might be caused due to low accuracy of cluster-level neighbor selection when the value of K is small. Hence, our future work will investigate how to enhance the quality of cluster-level neighbor selection.

Visualization. To gain some intuitive understanding of the performance of our proposed SiCL, we conduct a set of data visualization experiments on LTCC and VC-Clothes to visualize selected query samples with the top-10 best matching images in the gallery set, and display the visualization results in Figure 4 and Figure 5. Compared to CACL and SpCL, SiCL yields more precise matching results. The majority of the incorrect samples matched by other methods are in the same color as the query sample. These findings imply that SiCL can successfully learn more clothing invariance features and hence identify more precise matches.

7. Limitation and Future Work

In experiments, we construct a hierarchical neighbor structure using person silhouette masks and person images to drive the model learning in cross-clothes invariance. Experiments have shown that clothe-independent features can provide the correct guidance for the model. Therefore, it is promising to research generating higher quality person silhouette masks without supervision to further enrich the representation capacity, improve the stability and enhance the overall performance of the proposed framework.

Besides, pedestrian silhouette, person clothes-independent semantic sources comprise numerous categories, such as gait, skeleton. As the future work, it is interesting to investigate combine multiple types of sources to enhance the model performance.



Figure 4. Visualization of the top-10 best matched images on LTCC and VC-Clothes. We show the top-10 best matching samples in the gallery set for the query sample with CACL and our proposed SiCL. The images with frames in green and in red are the correctly matched images and mismatched images, respectively.



Figure 5. Visualization of the top-10 best matched images on LTCC and VC-Clothes. We show the top-10 best matching samples in the gallery set for the query sample with SpCL and our proposed SiCL. The images with frames in green and in red are the correctly matched images and mismatched images, respectively.